Fragment-based discovery of a new class of inhibitors targeting mycobacterial tRNA modification

Sherine E. Thomas[*1], Andrew J. Whitehouse[*2], Karen Brown[3,4], Juan M. Belardinelli[5], Ramanuj Lahiri[6], M. Daben J. Libardo[7], Pooja Gupta[1], Sony Malhotra[8], Helena I. M. Boshoff[7], Mary Jackson[5], Chris Abell [2], Anthony G. Coyne[2], Tom L. Blundell [§1], R. Andres Floto[3,4], Vítor Mendes [§1]

[1] Department of Biochemistry, University of Cambridge, 80 Tennis Court Road, Cambridge, CB2 1GA, UK

[2] Department of Chemistry, University of Cambridge, Lensfield Road, Cambridge, CB2 1EW, UK.

[3] MRC Laboratory of Molecular Biology, Francis Crick Avenue, Cambridge, CB2 0QH, UK.

[4] Cambridge Centre for Lung Infection, Royal Papworth Hospital, Cambridge, CB23 3RE, UK.

[5] Mycobacteria Research Laboratories, Department of Microbiology, Immunology and Pathology, Colorado State University, Fort Collins, Colorado, USA.

[6] National Hansen's Disease Program, Healthcare Systems Bureau, HRSA, DHHS, USA.

[7] Tuberculosis Research Section, Laboratory of Clinical Immunology and Microbiology, National Institute of Allergy and Infectious Disease, National Institutes of Health, 9000 Rockville Pike, Bethesda, Maryland 20892, USA.

[8] Birkbeck College, University of London, Malet Street, WC1E7HX, UK

[*] Contributed equally

[§] To whom correspondence should be addressed

Key words: Structure-guided; Fragment-based; Mycobacteriaceae; *Mycobacterium abscessus; Mycobacterium tuberculosis;* Cystic Fibrosis; TrmD.

Abbreviations: FBDD - fragment-based drug design; SAR - structure-activity relationship; NTM - non-tuberculous mycobacteria; SAM - S-adenosyl methionine; SAH - S-adenosyl homocysteine; LE - Ligand Efficiency; MIC – minimum inhibitory concentration.

Abstract

Translational frameshift errors are often deleterious to the synthesis of functional proteins as they lead to the production of truncated or inactive proteins. TrmD (tRNA-(N(1)G37) methyltransferase) is an essential tRNA modification enzyme in bacteria that prevents +1 errors in the reading frame during protein translation and has been identified as a therapeutic target for several bacterial infections. Here we validate TrmD as a target in *Mycobacterium abscessus* and describe the application of a structure-guided fragment-based drug discovery approach for the design of a new class of inhibitors against this enzyme. A fragment library screening followed by structure-guided chemical elaboration of hits led to the development of compounds with potent *in vitro* TrmD inhibitory activity. Several of these compounds exhibit activity against planktonic *M. abscessus and Mycobacterium tuberculosis*. The compounds were further active in macrophage infection models against *Mycobacterium leprae* and *M. abscessus* suggesting the potential for novel broad-spectrum mycobacterial drugs.

Introduction

Mycobacteria are a group of diverse organisms that include many important human pathogens. Within this group, *Mycobacterium tuberculosis*, the causative agent of Tuberculosis, is responsible for over 1.7 million deaths per year (Floyd et al., 2018). Nevertheless, *Mycobacterium abscessus*, a rapid growing species of nontuberculous mycobacteria (NTM), has recently emerged as a major threat to individuals with cystic fibrosis (CF) and other chronic inflammatory lung conditions (Bar-On et al., 2015; Sood and Parrish, 2017), with infection rates increasing around the World (Floto et al., 2016). *M. abscessus* is intrinsically resistant to most antibiotics and is consequently associated with extremely high treatment failure rates (Floto et al., 2016). There is therefore an urgent unmet need to develop new antibiotics.

Several structurally diverse, modified nucleosides, found at different locations of tRNAs, help in the maintenance of the reading frame and avoidance of translational frame-shift errors. Many such nucleoside modifications are found in regions near the anticodon, particularly at position 34 (the wobble position) and 37 (3' and adjacent to the anticodon) of tRNA (Ahn et al., 2003; Urbonavicius et al., 2001). TrmD, tRNA-(N(1)G37) methyltransferase, catalyzes the methylation of G_{37} (Guanosine at position 37) in prokaryotic tRNAs **(Figure 1A)**. This modified nucleotide N^1-methylguanosine at position 37 (m^1G_{37}) is present in tRNAs containing a $G_{36}G_{37}$ sequence in the anti-codon region from all three domains of life, where G_{37} is the base adjacent to the anticodon at the 3' end (Ahn et al., 2003; Bjork et al., 2001; Bjork et al., 1989). Mutations in *trmD* result in growth defects associated with increased translational frameshifting leading to defective protein production (Bjork et al, 1989; Urbonavicius, 2001). TrmD belongs to a distinct class of S-adenosyl-L-methionine (SAM)-dependent methyltransferases known as the SpoU-TrmD (SPOUT) RNA methyltransferase superfamily or Class IV methyltransferases. Proteins belonging to this family are structurally unique due to the absence of a consensus methyltransferase fold. TrmD and other proteins of the SPOUT

family consist of a deep trefoil knot architecture at the catalytic region, which provides an L-shaped pocket for binding of SAM. In eukaryotes however, G_{37} methylation is carried out by the enzyme Trm5, belonging to the Class I methyltransferase family (Anantharaman et al., 2002; Hori, 2017; Ito et al., 2015).

Previous research (Goto-Ito et al., 2009; Ito et al., 2015) has shown that TrmD and Trm5 have distinct substrate requirements with RNA. While Trm5 recognizes the overall L-shaped tertiary structure of tRNA possessing a G_{37} base, TrmD recognition involves mainly the D stem and anticodon stem loop of tRNA with $G_{36}G_{37}$ bases. Trm5 functions as a monomer and binds to SAM at the Rossmann fold region of the active site, in contrast to dimeric TrmD with a trefoil knot methyl donor binding region. Further, SAM adopts a unique bent conformation in TrmD as compared to the extended conformation in Trm5 and many other canonical methyltransferases. These distinct structural features, substrate requirements and ligand binding conformations provide the potential for designing novel and selective inhibitors of bacterial TrmD (Goto-Ito et al., 2017).

A previous drug discovery effort targeting *H. influenzae* TrmD (Hill et al., 2013) led to the development of selective inhibitors with potent biochemical activity against TrmD isozymes *in vitro*. However, these compounds only showed weak antibacterial activity when profiled against a range of Gram-positive and Gram- negative pathogens, including against recombinant strains of *E. coli* and *H. influenzae* debilitated in the AcrAB TolC efflux pumps (Hill et al., 2013). A recent drug discovery work was reported against *Pseudomonas aeruginosa* TrmD which reported potent inhibitors of this enzyme. However, the antibacterial activity of these was weak not only against *P. aeruginosa* but also against other bacteria including mycobacteria (Zhong et al., 2019).

Fragment-based drug discovery (FBDD) is a promising approach for the identification of new drugs, whereby the complexity of the chemicals screened is reduced by decreasing their

molecular weights (typically < 300 Da), which at the same time increases their promiscuity in binding targets. Initial fragment hits usually exhibit lower potency than the more complex drug-like molecules found in typical high-throughput screening compound libraries. However, such fragments bind by making well-defined and directional interactions, giving rise to high ligand efficient (LE) molecules. These fragments can be then chemically optimized into lead candidates, thereby more effectively exploring the chemical space available for binding to the target protein (Erlanson et al., 2016; Mendes and Blundell, 2016; Murray et al., 2014; Thomas et al., 2017). In this work we validate TrmD as a mycobacterial target and we describe the application of an FBDD approach to generate a new family of small-molecule inhibitors of *Mycobacterium abscessus* TrmD, having anti-microbial activities against a range of pathogenic mycobacteria.

Results

TrmD is essential for *M. abscessus*

Previous studies have demonstrated that *trmD* is essential in diverse bacteria including *M. tuberculosis*, where different transposon mutagenesis studies have shown that it is essential or that mutants had a growth defect (DeJesus et al., 2017; Griffin et al., 2011; Sassetti et al., 2003). However, confirmation of essentiality of *trmD* for *M. abscessus* was lacking. Three initial attempts to disrupt the *trmD* gene of *M. abscessus* subsp. *massiliense* CIP108297 by homologous recombination using a recombineering approach proved unsuccessful. To determine whether the *trmD* gene is required for *M. abscessus* growth, allelic replacement experiments were repeated in the background of a *M. abscessus* subsp. *massiliense* CIP108297 merodiploid expressing a second copy of the *trmD* gene from the integrative plasmid pMV306H::*trmD*, and in a control *M. abscessus* subsp. *massiliense* CIP108297 strain harbouring an empty pMV306H plasmid. Analysis of over 100 candidate mutants in each

background from two independent experiments showed that the endogenous chromosomal copy of *trmD* could be knocked-out in the presence of an extra-copy of the gene but not in *M. abscessus* cells carrying an empty plasmid (**Figure 1B**), thus confirming *trmD* essentiality for *M. abscessus* growth.

M. abscessus TrmD: overall structure and ligand binding

We determined the crystal structures of *M. abscessus* TrmD in apo form at 1.60 Å resolution (PDB code **6NVR**) as well as in complex with SAM and S-adenosyl-L-homocysteine (SAH) at 1.67 Å and 1.48 Å resolutions, respectively (PDB codes **6NW6** & **6NW7**). The crystals belong to space group $P2_12_12_1$ and consist of a homodimer in the asymmetric unit. Each non-crystallographic two-fold symmetry-related protomer of TrmD interacts in an antiparallel manner and consists of two domains: a larger N-terminal domain spanning residues 1-161 and a smaller C-terminal helical domain (162-242) connected by a flexible inter-domain linker. The two domains of individual protomers do not contact each other and the inter-domain region is largely disordered with residues 163-177 not clearly visible in the apo structure (**Figure 1 C & D).**

The SAM binding region of TrmD is located at the base of the N-terminal domain and consists of a deep trefoil knot architecture, made of three distinct untwisted loop regions. The trefoil knot of *M. abscessus* TrmD is made up of a cover loop spanning residues ^{84}TPAG^{87} between strand β3 and helix α4 leading to the wall loop at the edge of the methionine pocket containing residues ^{109}GRYEGID^{115} between β4 and helix α5. This loop then crosses over and form the bottom loop formed of residues 132-140 that encompasses the SAM adenine ring between strand β5 and helix α6 **(Figure 2 A & B).** SAM and SAH occupy the deep trefoil-knot active site at the base of the N-terminal region and adopt an L-shaped bent conformation as previously observed with other TrmD orthologs (Christian et al., 2016; Koh et al., 2017). Both SAM and

SAH form an extensive hydrogen-bonding network in this region along with hydrophobic and π-interactions. The adenine ring of SAM and SAH is sandwiched between the cover loop (residues 84-91) and bottom loop (residues 132-140) of the knot with the adenine N1 and N7 forming hydrogen-bond contacts with the backbone amide-nitrogen atoms of Ile133 and Leu138, respectively, while N6 forms additional hydrogen bonding contacts with the backbone carbonyl oxygen atoms of Gly134 and Tyr136 of the bottom loop (**Figure 2 B & C**).

The ribose and methionine moieties of SAM and SAH interact with the wall (residues 109-115) and bottom loops of the knot. The hydroxyl oxygen atom (O2') of the ribose ring forms a hydrogen bond with the backbone amide of Gly109. The other hydroxyl oxygen atoms O3' and the O4' of ribose forms weak hydrogen bond contacts with the backbone nitrogen atoms of Gly113 and Gly140 respectively. The methionine and homocysteine moieties further extends into the active site groove formed between the cover and wall loops, making further hydrogen-bonding interactions in this region (**Figure 2 B & C**).

A structural superposition of the apo and SAM bound forms of TrmD reveals the wall loop (residues ^{109}GRYEGID^{115}) undergoing a switch in conformation leading to a movement of about 5 Å, when measured at the Cα of Tyr111, to the outer edge of subunit A. This conformational flip of the wall loop from apo form to SAM-bound form and the subsequent change in positions of residues 110 to 113 help to accommodate the methionine moiety of the methyl donor (**Figure 2 A & B**).

Fragment Screening, hit validation and clustering of fragments

Having examined the conformational changes and binding interactions at the *M. abscessus* TrmD catalytic site, we initiated a structure-guided fragment-based drug discovery effort targeting *M. abscessus* TrmD by screening an in-house library of 960 small molecule fragments. The preliminary screening was performed using differential scanning fluorimetry (DSF),

resulting in 53 hits within a thermal shift cut-off value of 3 standard deviations from the negative control, consisting of TrmD protein in the absence of any ligand. These hits were then selected for subsequent experiments by X-ray crystallography. Apo crystals of *M. abscessus* TrmD were soaked with each of the 53 fragments in individual experiments. The resulting crystal structure determinations helped in the characterization of the binding modes of 27 fragments (**Figure S3**).

All of the 27 fragments, validated by X-ray crystallography, were found to occupy the TrmD SAM site. These fragments can be clustered into three groups based on their mode of binding at this site (**Figure 2 D & S3**). **Cluster 1** consists of 12 fragments that bind exclusively to the sub-pocket that accommodates the adenine ring of SAM, where it engages residues within the cover loop and bottom loop of the trefoil knot. These fragments recapitulated many of the hydrogen bonding and π-interactions of SAM adenine moiety, as shown in the example (**Figure 2 D & S3)**. These interactions include hydrogen-bond contacts to the side chain of Ser132 and to the backbone amides of Ile133, Gly134, Try136 and Leu138.

The **second cluster** consists of 12 further fragments that occupy the entire adenosine region of the TrmD active site, thus extending from adenine towards the ribose-binding pocket of the active site. These fragments, in addition to retaining several adenine moiety contacts, also interact with the wall loop residues, forming hydrogen bonds to the backbone amides of Tyr111 and Gly109 and water-mediated hydrogen bonds as shown in the example (**Figure 2 D & S3).** **Cluster 3** consists of three fragments that extend beyond the TrmD adenosine site, thus reaching the methionine-binding region of the pocket. One of these fragments, fragment **8** stretched further into the groove formed between the cover and wall loops of the trefoil knot, thus engaging additional hydrogen bonding contacts with the side chain of Thr84 and the back bone amide of Gly109 in this region (**Figure 2 D & S3).**

Fragment merging & hotspot mapping for chemical elaboration

Two of the above 27 fragment hits, fragments **23** (K_d 0.17 mM, LE 0.37) and **24** (K_d 0.26 mM, LE 0.41), were chosen for further chemical development by a fragment-merging strategy. The choice of fragments for subsequent chemical optimization was based on a number of criteria, such as binding affinity, ligand efficiency, synthetic tractability and their ability to make key binding interactions at the TrmD SAM binding site. Fragment **23** occupies the adenosine binding region of the TrmD AdoMet site, with its aminopyrazole ring making hydrogen bond contacts to the backbone amides of Tyr136 and Leu138 and the amino group making further hydrogen bonds with the backbone carbonyl oxygen of Gly134 and the side chain of Ser132, respectively. The 4-methoxyphenyl ring of the fragment extends into the ribose binding site engaging hydrophobic and π-interactions with the residues of the cover and wall loops. (**Figure 3A & S3).**

The indole ring of fragment **24** also occupies the ribose pocket where it forms a water-mediated interaction with backbone amide nitrogen of Leu138. The 4-methoxyphenyl and indole ring systems of fragments **23** and **24** overlap perfectly, while the 6-boronic acid group of fragment **24** partially extends into the SAM adenine pocket and makes hydrogen bonds with backbone amides of residues Tyr136 and Leu138 and further water-mediated hydrogen bond contacts to the backbone amides of Val131, Ile133, Gly134 and the side chain hydroxyl group of Ser132 (**Figure 3A & S3**). Compound **AW1** (K_d 0.11 mM, LE 0.36), formed by merging the two fragments, adopts a similar conformation to that of the original fragments in the TrmD SAM site, as shown in **Figures 3 B & C**, thereby providing a new chemical scaffold for further structure-guided development.

To aid the structure-guided lead discovery, the binding propensities of TrmD protein to ligands were further examined using the hotspot-mapping program developed by Radoux and co-workers (Radoux et al., 2016) . Hotspots are areas within the protein that provide relatively

large contributions to the overall binding affinity of ligands (Hajduk et al., 2005; Ichihara et al., 2014). This is usually mediated by the displacement of water molecules having restricted freedom owing to their location within a hydrophobic cavity or close to a patchwork of hydrogen bonds and lipophilic amino acid side chains, thus compensating for the loss of entropy on binding. These regions not only satisfy the minimum binding requirement for fragments but also maintain the original fragment binding interactions when elaborated (Radoux et al., 2016). While the observed fragment hits and the corresponding merged compound **AW1** satisfy many of the predicted protein-hotspot interactions, the map at lower contours also suggests "warm spots" providing further interactions stabilise elaborated fragments, and sometimes allowing them to reach other hotspots that are not yet explored. As shown in the example (**Figure 3 D**), **AW1** occupied the hotspot 1 at the base of the TrmD active site, where it satisfies the hydrogen-bond donor hotspot by providing donating groups for interaction with the backbone amide oxygen atoms of Gly134 and Tyr136. The merged compound **AW1** also engages the pyrazole nitrogen atom in the acceptor hotspot in this region when it forms a hydrogen bond with the backbone NH of Leu138 (**Figure 3 D**). The compound could be elaborated further towards the donor region at the methionine end of the active site by engaging water-mediated hydrogen bonds to the backbone amide groups of Asn139 and Tyr111, followed by further extension to the second hotspot region at the top of the active site. The second hotspot is characterized by a large hydrophobic patch surrounded by the acceptor hotspot mediated by the backbone amide group and side chain of Glu180. A second approach to fragment elaboration is by growing further upwards from the hydrophobic region of hotspot 2 over to the donor region mainly mediated by backbone oxygen atom and side chains of Glu112 as illustrated in **Figure 3 D**.

Structure-based lead optimization of merged compounds

A structure guided elaboration of the merged compound **AW1** (K_d 110 µM, IC_{50} 226 µM, LE 0.36) was carried out, initially utilizing the indole nitrogen as a vector for growth. The addition of a 2-picolyl moiety successfully increased the affinity of **AW1** by an order of magnitude in compound **AW2** to a K_d of 12.3 µM and IC_{50} 32.5 µM (**Table 1**). The methylene linker attached to the indole nitrogen of **AW2** allowed the added pyridyl ring to occupy the region defined by Pro85, Glu112, Val137, Arg154 and Glu180 **(Figures 3E & 4A).**

The affinity of **AW2** was further improved by the addition of a nitrile group on the 4-position of its pyrazole ring, extending into the narrow space between residues ^{83}PTP^{85} of the cover loop and ^{131}VSI^{133} of the bottom loop respectively **(Figure 4 A & B). AW3** was a significant improvement on **AW2**, with the addition of two heavy atoms affording a 20-fold decrease in K_d (12.3 µM to 0.50 µM) and IC_{50} (32.5 µM to 0.31 µM), increasing the ligand efficiency to the level of the original merged compound (**Table 1**). The X-ray crystal structure of TrmD in complex with **AW3** shows that the original fragment contacts have been retained, with the **AW3** aminopyrazole ring orienting itself in a similar manner to **AW1**, retaining its hydrogen bonding contacts to the side chain of Ser132 and backbones of Gly134, Tyr136 and Leu138. In addition, the nitrile substitution of **AW3** seems to have strengthened the interactions at the active site region between residues ^{83}PTP^{85} and ^{131}VSI^{133} by engaging in additional hydrogen bond contact with the backbone NH of Ile133 **(Figure 4B).**

Further elaboration was carried out from the 5-position of the pyridyl ring of **AW3** through the attachment of a pyrrolidine ring via another methylene linker, with **AW4** affording and additional ~5-fold improvement in affinity to 87 nM (**Table 1**). Simplification of the scaffold of **AW4** by replacement of its pyridyl ring with a phenyl ring in **AW5** was tolerated with a two-fold improvement in affinity (87 nM to 27 nM) and an increase in ligand efficiency (0.32 to 0.34). The X-ray crystal structure of **AW5** shows the pyrrolidine ring occupying the binding

site in two conformations, depending on the active site, there by engaging either Glu112 or Glu180 in an electrostatic interaction **(Figure 4 C & D).** Removing the nitrile group on the pyrazole ring in compound **AW6 (Figure 5A)**, substantially weakened the affinity ~15-fold to 0.49 µM while the biochemical assay showed an even greater impact of close to ~50-fold increase in IC_{50}, demonstrating the importance of having the nitrile extending into the cavity between residues ^{83}PTP^{85} of the cover loop and ^{131}VSI^{133} of the bottom loop, respectively. Further attempts to explore the active site region bordered by the Ala176 to Glu180 loop by replacing the pyrrolidine ring of **AW5** with an N-methyl piperazine (compound **AW7**) but keeping the nitrile group on the pyrazole ring, showed a slight worsening of both affinity and IC_{50} possibly due to the slight change (0.3 Å) in the position of the nitrile group in comparison to that of **AW5** there by diminishing the hydrogen bonding contact with backbone amide of Thr84 (**Figure 5 B** & **S6**).

TrmD lead compounds have anti-mycobacterial activity

The compounds were further examined for their ability to inhibit bacterial growth. While the initial fragment hits of TrmD and the early stage compounds elaborated from the fragments exhibited low levels of growth inhibition up to 250 µM (data not shown), compounds in later stages of development, following fragment merging, showed promising activity against *M. abscessus* and *M. tuberculosis* (**Table 2**). The MIC of the TrmD lead compounds against *M. abscessus* were identical and most of the lead molecules exhibited much higher inhibition against *M. tuberculosis* than *M. abscessus* **(Table 2).** Surprisingly, **AW6,** in which the nitrile group was removed, was the least active lead compound in the *in vitro* TrmD assays, with ~15-fold worse K_d and ~50-fold higher $IC_{50,}$ but showed similar MICs when compared to the other two compounds. Additionally, the substitution of the pyrrolidine ring of **AW5** with an N-methyl piperazine motif in **AW7** that also showed a slight worsening of activity *in vitro* against

TrmD, displayed a 2-fold improvement in the MIC compared to **AW5** against *M. tuberculosis*, but such effect wasn't observed in *M. abscessus* **(Table 2).** Two of the lead molecules (**AW6** and **AW7**) were then tested against a wider panel of nontuberculous mycobacteria (NTMs) **(Table 2).** The obtained MICs revealed that the compounds display limited inhibitory activity across most NTMs tested except for *Mycobacterium terrae* where MICs are better than for *M. abscessus*. Given the high percentage sequence identity of TrmD across mycobacterial species **(Figure S1),** it was expected to observe growth inhibition against some of these organisms. However, given that different mycobacteria respond very differently to the same drug (Li et al., 2013) due to differential permeability, retention, and metabolism of compounds, the variation of MIC observed for our lead compounds is in line with the variation observed for most of the drugs used against these organisms (Li et al., 2013; Scherr et al., 2016).

TrmD lead compounds kill intracellular *M. abscessus* and *M. leprae*

We assessed the cytotoxicity effect of **AW6** and **AW7** using lactate dehydrogenase (LDH) release assay. At or below 150 µM, neither compound caused cellular toxicity on human macrophages (**Figure S4).** The compounds were then evaluated in *M. abscessus*-infected human macrophages. Both compounds showed activity in the macrophage infection model, with **AW7** performing better than in the *in vitro* assays. At 25 µM **AW6** showed a ~82 % decrease in CFUs while **AW7** at the same concentration showed a 95 % reduction in CFUs compared to the no drug control after 48h incubation (**Figure 5C**). However, only **AW7** demonstrated a bactericidal effect with a -0.8 log change after 48h incubation (**Figure S7**).

The best lead molecule (**AW7**) was further tested against *M. leprae* maintained intracellularly in murine bone marrow macrophage. Relative inhibition of β-oxidation rates were measured using radiorespirometry assay after 7 days of incubation. The results show that **AW7** at 6.2 µM was able to inhibit *M. leprae* radiorespirometry by ~54 % when compared to the no-drug

control and by ~89 % at 25 µM, which is similar to rifampicin inhibition at 2.4 µM (91%) (**Figure 5D**). While axenically-maintained *M. leprae* showed only a 15% reduction of radiorespirometry at 25 µM and no effect at 6.2 µM following a similar trend to what was observed for *M. abscessus* with the highest activity for the compound being observed in the macrophage infection model (**Figure S5**).

Discussion

TrmD (tRNA-(N(1)G37) methyltransferase) is an essential tRNA modification enzyme in bacteria that prevents translational frame-shift errors by methylation of a guanosine base at position 37 of tRNAs containing $G_{36}G_{37}$ bases at the anti-codon region. This enzyme was found to be essential in *M. tuberculosis* and other organisms but direct confirmation for *M. abscessus* was lacking. This work has confirmed the essentiality of *trmD* for *M. abscessus* subsp. *massiliense* growth, validating TrmD as a drug discovery target for this organism.

A fragment-based drug discovery effort targeting *M. abscessus* TrmD was undertaken by screening a library of 960 fragments by DSF and resulted in 53 preliminary hits. Of these, 27 were subsequently validated by X-ray crystallographic studies of the TrmD-fragment complexes. The resulting fragments can be classed into three clusters corresponding to their different binding modes in the TrmD SAM binding site. The determination of high-resolution crystal structures informed structure-guided drug discovery and allowed us to select and develop a series of compounds by merging two fragments fragment **23** and **24**. Chemical elaboration progressed from the indole nitrogen of the merged compound and allowed the synthesis of potent *M. abscessus* TrmD inhibitors. While the addition of a nitrile group on the 4-position of pyrazole also gave rise to a large increase in affinity. Subsequent SAR development by addition of benzyl and pyridine ring systems helped in achieving chemical scaffolds with improved ligand efficiencies. Structure-guided elaborations of these scaffolds

using piperidine and pyrrolidine moieties led to several low nano-molar *M. abscessus* TrmD inhibitors demonstrating a ~4000-fold improvement of *in vitro* affinities from the initial fragments.

The lead compounds reported in this work, exhibited bactericidal effect on *M. abscessus*, *M. tuberculosis*, and *M. terrae*. Furthermore, compound **AW7** showed bactericidal intracellular activity against *M. abscessus* and was also a potent inhibitor of intracellular *M. leprae*. The compounds reported here are the first TrmD inhibitors reported in the literature with strong bactericidal activity against mycobacteria. However, we observe a poor correlation between K_d/ IC_{50} and MIC for the lead compound, **AW6**, the weakest of the lead compounds presenting similar MIC to the other compounds against most of the species tested. Furthermore, the compounds have nanomolar affinities against *M. abscessus* TrmD and likely similar affinities for other mycobacterial TrmD, given the very high sequence identity shared between the TrmD orthologues (**Figure S1**), while their MICs are ~35-3000 fold worse across the several NTMs tested. This poor correlation and variation across different mycobacterial species suggests differential effects of compound permeability, retention, and/or metabolism on *in vivo* activity. Similar results were found by others in a recent phenotypic screen of 129 TB active and 271 non-TB active compounds against *M. abscessus* which revealed that only a small subset (12 compounds) from the TB-active group and just one compound from the non-TB active group were effective against *M. abscessus* (Low et al., 2017). Nevertheless, our results with macrophage infection models, both with *M. leprae* and *M. abscessus*, show the potential of these molecules to be further optimized. The preliminary toxicity study of the lead molecules **AW6** and **AW7** using a lactate dehydrogenase (LDH) assay further showed no significant cytotoxicity on primary human macrophages.

Most currently-used antibiotics that target microbial protein synthesis act either by interacting with ribosomal sub-units (amino glycosides, tetracyclines, macrolides etc) or *via* inhibiting

mRNA synthesis (rifamycins) and elongation (actinomycin) (Kohanski et al., 2010). This study represents a proof of concept for the development of a new class of antibiotics targeting bacterial tRNA modification with potent bactericidal activities. Furthermore, the results presented in this work suggest the potential to develop novel mycobacterial drugs targeting bacterial tRNA methylation by TrmD.

Materials & Methods

Expression and purification of full length *M. abscessus* TrmD

E. coli BL21 (DE3) strain containing AVA0421 plasmid with an N-His-3C Protease site-TrmD full-length insert, kindly provided by the Seattle Structural Genomics Consortium, (Baugh et al., 2015) was grown overnight at 37°C in LB-media containing Ampicillin (100 µg/ml). This seed stage culture was used to inoculate 6 shake flasks containing 1 L each of 2XYT media with Ampicillin (100 µg/ml) until optical density (A_{600nm}) reached 0.6. The expression of recombinant construct was induced by the addition of Isopropyl β-D-1-thiogalactopyranoside (IPTG) to a final concentration of 0.5 mM and further allowed to grow at 18 °C for 16 h.

Isolation of cells & lysis: Cells were harvested by centrifugation at 4°C for 20 min at 5000 g and the pellet was re-suspended in buffer A (25 mM Hepes pH 7.5, 500 mM NaCl, 5% Glycerol, 10 mM $MgCl_2$, 1 mM TCEP, 20 mM Imidazole). 0.1 % Triton (Sigma), 10 µg/mL DNaseI, 5 mM $MgCl_2$, and 3 protease inhibitor cocktail tablets (New England Biolabs) were added to the cell suspension. The cells were lysed in an Emulsiflex (Glen Creston) and clarified the lysate by centrifugation at 4°C for 40 min at 25,568 g.

Immobilized Metal Affinity Chromatography: The clarified lysate was filtered using a 0.45 µm syringe filter and passed through a pre-equilibrated (with buffer A), 10 mL pre-packed nickel-sepharose column (HiTrap IMAC FF, GE Healthcare). The column was washed with 5 column volumes of buffer A and the bound protein was eluted as 4x 10ml elutes using buffer B (25

mM Hepes pH 7.5, 500 mM NaCl, 5% Glycerol, 1 mM TCEP, 500 mM Imidazole). The protein was analyzed on a 15% SDS-PAGE gel. *Dialysis*: Elutes from Hi-Trap IMAC column were pooled, added 3C Protease in the ratio of 1: 50 mg (protease: protein) and subjected to dialysis against 2 L of buffer C (25 mM Hepes pH 7.5, 500 mM NaCl, 5 % Glycerol, 1 mM TCEP) overnight at 4°C.

Protein, after overnight dialysis and cleavage of N-His tag, was passed through a pre-equilibrated (buffer A) 5 mL HiTrap IMAC FF Nickel column (GE Healthcare).

Size Exclusion Chromatography: The flow through from the above column was concentrated to 3 mL using a 10 kDa centrifugal concentrator (Sartorius Stedim) and loaded onto a pre-equilibrated (with buffer D: 25 mM Hepes pH 7.5, 500 mM NaCl, 5 % Glycerol) 120 ml Superdex200 16/600 column (GE Healthcare). 2 mL fractions were collected and analyzed on a 15% SDS-PAGE gel. Fractions corresponding to pure TrmD protein were pooled and concentrated to 25mg/ml, flash frozen in liquid nitrogen and stored at -80°C. Identity of the purified protein was further confirmed by MALDI fingerprinting.

Crystallization of apo form of full length *M. abscessus* TrmD

M. abscessus TrmD apo crystals were grown in 48-well sitting drop plates (Swiss CDI) in the following condition: 0.08 mM Sodium cacodylate pH 5.8 to 6.8, 1– 2 M Ammonium sulphate. 24 mg/mL of the protein in storage buffer (25 mM Hepes pH 7.5, 500 mM NaCl, 5% Glycerol) at drop ratio 1 μL: 1 μL (protein: reservoir respectively) were set up and equilibrated against 70 μL reservoir.

Soaking of TrmD native crystals with fragments and ligands

Crystals for this experiment were grown at 19°C in 48-well sitting drop plates (Swiss CDI) in the following condition: 0.08 mM Sodium cacodylate pH 6.5 to 7.0, 1–2 M Ammonium

sulphate, 20 mg/mL of the protein in storage buffer (25 mM Hepes pH 7.5, 500 mM NaCl, 5% Glycerol) at drop ratio 1 μL: 1 μL were set up and equilibrated against 250 μL reservoir. Further, the crystals were picked and allowed to soak in a 4 μL drop containing reservoir solution and 10 mM fragments/compound (in DMSO) which was then equilibrated against 700 μL of the corresponding reservoir solution overnight at 19°C in 24-well hanging drop vapour diffusion set up.

Co-crystallization of TrmD protein with SAM/ SAH/ AW6/ AW7

2mM-5mM final concentration of compound in DMSO/water was added to 20 mg/mL of TrmD protein, mixed and incubated for 2 h on ice. Crystals were grown in the following condition: 0.08mM Sodium cacodylate pH 6.5 to 7.0, 1M– 2M Ammonium sulphate or in sparse matrix screens: Wizard 1&2 (Molecular Dimensions), Wizard 3&4 (Molecular Dimensions), JCSG +Suite (Molecular Dimensions). The crystallization drops were set up at a protein to reservoir drop ratio of 0.3 μL: 0.3 μL, in 96-well (MRC2) sitting drop plate, using Mosquito crystallization robot (TTP labtech) and the drops were equilibrated against 70 μL of reservoir at 19°C.

X-ray Data Collection and Processing

The TrmD apo/ligand-bound crystals were cryo-cooled in mother liquor containing 27.5% ethylene glycol. X-ray data sets were collected on I04, I02, I03, I04-1 or I24 beamlines at the Diamond Light Source in the UK, using the rotation method at wavelength of 0.979 Å, Omega start: 0°, Omega Oscillation: 0.1-0.2^{o}, Total oscillation: 210-240 ^{o}, Total images: 2100-2400, Exposure time: 0.05-0.08 s. The diffraction images were processed using AutoPROC (Vonrhein et al., 2011), utilizing XDS (Kabsch, 2010) for indexing, integration, followed by POINTLESS (Evans, 2011), AIMLESS (Evans and Murshudov, 2013) and TRUNCATE

(French, 1978) programs from CCP4 Suite (Winn et al., 2011) for data reduction, scaling and calculation of structure factor amplitudes and intensity statistics. All TrmD crystals belonged to space group $P2_12_12_1$ and consisted of two protomers in the asymmetric unit.

Structure Solution and refinement

The *Mycobacterium abscessus* TrmD Apo structure was solved by molecular replacement using PHASER (McCoy et al., 2007) with the atomic coordinates of *Mycobacterium abscessus* TrmD at 1.7 Å (PDB entry: 3QUV Seattle Structural Genomics Consortium for Infectious Diseases) as search model and TrmD ligand bound structures were solved by molecular replacement with the atomic coordinates of the solved *Mycobacterium abscessus* TrmD Apo structure (PDB entry: 6NVR) as search model. Structure refinement was carried out using REFMAC (Murshudov et al., 2011) and PHENIX (Adams et al., 2010).

The models obtained were manually re-built using COOT interactive graphics program (Emsley and Cowtan, 2004) and electron density maps were calculated with $2|F_o|- |F_c|$ and $|F_o| - |F_c|$ co-efficients. Positions of ligands and water molecules were located in difference electron density maps and OMIT difference maps $|mFo - DFc|$ (Hodel, 1992) were calculated and analysed to further verify positions of fragments and ligands. The corresponding statistics and omit maps are presented in supplementary data **Table S1** and **Figure S8**.

Differential scanning fluorimetry (DSF)

DSF were carried out in a 96-well format with each well containing 25 µL of reaction mixture of 10 µM TrmD protein in buffer (50 mM Hepes pH 7.5, 500 mM NaCl, 5% glycerol), 5 mM compound, 5% DMSO and 5X Sypro orange dye. Appropriate positive (Protein, DMSO and SAM) and negative (Protein, DMSO only) controls were also included. The measurements were performed in a Biorad-CFX connect thermal cycler using the following program: 25°C

for 10 mins followed by a linear increment of 0.5°C every 30 sec to reach a final temperature of 95°C. The results were analyzed using Microsoft excel.

Isothermal Titration Calorimetry (ITC)

ITC experiments to quantitate binding of ligands to *Mycobacterium abscessus* TrmD were done as described in **(Whitehouse *et al.* 2019)** using using Malvern MicroCal iTC200 or Auto-iTC200 systems at 25 °C. The protein for ITC was dialysed overnight at 4°C in storage buffer (50 mM Hepes pH 7.5, 500 mM NaCl, 5% glycerol) the same buffer was used for preparing the ligand solutions. Composition of buffer components and other constituents like DMSO were kept constant in both protein and ligand solutions. Ligands to buffer titrations were subtracted in all cases and experiments were repeated at least twice. Data were analysed using the Origin software (OriginLab, Northampton, MA, USA).

Biochemical activity assays

Assays for quantifying TrmD methylation reactions were carried out in 20uL reactions consisting of 6.25 μM SAM, 0.1 μM TrmD and 6.25 μM tRNA in the presence of 0-500 μM compounds in serial dilutions using assay buffer containing 50 mM Tris-HCl pH 7.5, 10 mM $MgCl_2$, 24 mM NH_4Cl, 5% DMSO and 1 mM DTT in nuclease free water. tRNA sequences were identified from the *M. abscessus* genome sequence using tRNAscan-SE algorithm, (Lowe and Chan, 2016; Lowe and Eddy, 1997). The substrate $tRNA^{Pro}$ for the assay was purchased commercially from Integrated DNA technologies (USA). The reactions were carried out for 1 h at room temperature followed by addition of 20 mM EDTA to stop the reactions. Each of the 20 uL samples were diluted ten-fold with the UPLC mobile phase solvent A (0.1%formic acid in water), centrifuged for 10 min at 13,000 g, to remove any precipitates, and the supernatant was aliquoted into 96-well plates. 40uL samples were then injected into Acquity UPLC

(Waters) T3 1.8 µM column and eluted using a gradient elution consisting of Mobile Phase A: 0.1% Formic acid in water and mobile phase B: 0.1% Formic acid in 100% Methanol for 4 min. The absorbance was monitored using a photodiode array (PDA) detector (Waters) at wavelength range of λ: 220– 500 nm. All reactions were carried out in triplicate. The blank corrected data were analysed using Microsoft excel and non-linear regression analysis for IC_{50} determination were done using Graph Pad prism version 7.00, GraphPad Software, La Jolla California USA.

Mycobacterial strains used and MIC measurements

The following mycobacterial strains were used: *Mycobacteroides abscessus subspecies abscessus* (ATCC 19977) transformed with pmv310 plasmid expressing Lux ABDCE operon, grown in Middlebrook 7H9 broth supplemented with ADC (Sigma,UK) and *M. tuberculosis* ΔleuD ΔpanCD (Bleupan) (Sampson et al., 2004) transformed with pSMT1 expressing Lux AB and GFP, grown in Middlebrook 7H9 broth supplemented with 0.5% glycerol, 0.05% Tween 80 (removed for 24 h prior to experiments), 10% OADC (BD), 0.05 mg/ml L-leucine, and 0.024 mg/ml calcium pantothenate, Hygromycin and Zeocin (removed for 24 h prior to experiments). All the other NTM strains are clinical isolates. Minimum Inhibitory Concentrations (MIC) were determined for mycobacteria according to the Clinical and Laboratory Standards Institute (CLSI) method M07-A9. Briefly, mycobacteria were grown to optical density (A_{600nm}) of 0.2-0.3 in liquid culture and 1 x 10^5 bacteria were added to each well of 96-well plates containing serial dilutions of compound (400, 200, 100, 50, 25, 12.5, 6.3, 3.1, 1.6, 0.8, 0.4, 0 µM), in triplicate wells per condition, and incubated at 37ºC until growth was seen in the control wells.

Macrophage infection study

Blood samples were donated by healthy volunteers who had undertaken informed consent in accordance with local Research Ethics Committee approval. Peripheral blood mononuclear cells were isolated from citrated peripheral blood samples by density gradient separation using Lympholyte (Cedarlane Labs), and subsequent $CD14^+$ positive selection using the MACS Miltenyi Biotec Human CD14 microbead protocol (Miltenyi Biotec). $CD14^+$ cells were differentiated in to macrophages using recombinant human granulocyte-macrophage colony-stimulating factor (200ng/mL GM-CSF) and recombinant human interferon gamma (50ng/ml IFNγ) (Peprotech) in standard tissue culture DMEM media containing fetal calf serum, penicillin and streptomycin. Following removal of antibiotics, macrophages were infected at a multiplicity of infection of 10:1 with *M abscessus* 19977 for 2 h, washed in sterile phosphate buffered saline, and then incubated in DMEM media with FCS and 25 µM of compound for 24 and 48 h. At the given time points, supernatant was saved for cell cytotoxicity studies, and *M abscessus* survival within the macrophages calculated by macrophage lysis in sterile water, and colony forming unit calculation on Columbia Blood Agar plates (VWR BDH).

Cytotoxicity

Lactate dehydrogenase (LDH) was measured as a biomarker for cellular cytotoxicity using the Pierce LDH Cytotoxicity Assay Kit. Cell supernatant was measured at 2, 24 and 48 hours post infection according to the kit protocol.

Nude mouse derived *M. leprae*

Mycobacterium leprae (isolate Thai-53) was maintained in serial passage in the foot pads of athymic nude mice (Envigo, US.). Mice were inoculated in the plantar surface of both hind feet with 5×10^7 fresh, viable nude mice derived *M. leprae*. When the mouse foot pads became

moderately enlarged (at ~ 5 - 6 months), they were harvested for intracellular *M. leprae* as described previously (Truman and Krahenbuhl, 2001), washed by centrifugation, re-suspended in medium, enumerated by direct count of acid fast bacilli according to Shepard's method (Shepard and McRae, 1968), held at 4 ^{o}C pending quality control tests for contamination and viability (Truman and Krahenbuhl, 2001). Freshly harvested bacilli were always employed in experiments within 24 h of harvest.

***M. leprae* axenic culture**

Freshly harvested nude mouse foot pad derived *M. leprae* were suspended in modified 7H12 medium, **AW7** was added at different concentrations (100 μM – 6.25 μM) and were incubated for 7 days at 33°C. Media only and rifampin (Sigma, USA) at 2.4 μM were used as negative and positive controls. Following incubation aliquots of **AW7** treated and control *M. leprae* were processed for radiorespirometry (RR) as described previously (Lahiri et al., 2005).

***M. leprae* macrophage culture**

Bone marrow cells were obtained aseptically from both femurs of female BALB/c mice and cultured on plastic cover slips in Dulbecco modified Eagle media (DMEM, Life Technologies, USA) supplemented with 10% v/v fetal calf serum (Life Technologies), 25 mM/L HEPES (Sigma, USA), 2 mM/L glutamine (Sigma, USA), 50 μg/mL ampicillin (Sigma, USA) and 10 ng/mL of recombinant murine macrophages colony stimulating factor (R &D Systems, USA) for 6 - 7 days at 37°C and 5% CO_2. The cells were infected with freshly harvested nude mice foot pad derived live *M. leprae* at a multiplicity of infection (MOI) of 20:1 overnight at 33°C and then washed to remove extracellular bacteria. **AW7** was added at different concentrations (100 μM – 6.25 μM) and the cells were incubated for 7 days at 33°C. Media only and rifampicin at 2.4 μM were used as negative and positive controls. **AW7** treated and control cells were

lysed with sodium dodecyl sulfate (SDS, 0.1% w/v, Sigma, USA) and the intracellular *M. leprae* processed for radiorespirometry (Lahiri et al., 2010).

Radiorespirometry

Metabolism of a suspension of *M. leprae* was measured by evaluating the oxidation of ^{14}C-palmitic acid to $^{14}CO_2$ by radiorespirometry as described previously (Franzblau, 1988). Levels of captured $^{14}CO_2$ is proportional to the rate of ^{14}C-palmitic acid oxidation and used as an indicator of *M. leprae* viability. In the present study the 7th day cumulative counts per minute (CPM) were recorded and percentage inhibition of metabolism determined as compared to no drug control. Statistical significance between treatment groups and no drug control were determined by Student's t-test and $P < 0.05$ is considered as significant.

Figure Legends

Figure 1: A) TrmD reaction scheme illustrated with $tRNA^{Leu}$ CAG as substrate **B)** Allelic replacement at the *trmD* locus of *M. abscessus*. Candidate *trmD* mutants were analyzed by PCR using a set of primers annealing outside the allelic exchange substrate. Lanes 1 to 6 show *M. abscessus subsp. massiliense* CIP108297 clones harboring the pMV306H::*trmD* plasmid whose endogenous chromosomal *trmD* locus was replaced by the Str cassette (expected size of the PCR fragment is 4,200 bp). Lane 7 shows the amplification product of the *trmD* locus in wild-type *M. abscessus subsp. massiliense* CIP108297 (expected size of the PCR fragment is 2,571 bp). MWM, molecular weight marker. **C)** TrmD homodimer (PDB code 6NVR) with domain architecture illustrated. Protomers 1 and 2 are represented in brown and green ribbon diagrams respectively. **D)** TrmD protomer is coloured and illustrated based on secondary structure elements. The disordered inter-domain linker is shown as black dotted lines.

Figure 2: **A)** Structural superposition of TrmD apo form (white) and TrmD SAM bound form (blue), PDB code 6NW6, with the trefoil-knot active site involving: cover loop (residues 84-87) shown in dark blue and bottom loop (residues 132-140) in magenta and wall loop (residues 109-115) in green and residues corresponding to each loop are shown in line representation **B)** Conformational flip of the wall loop (residues ^{109}GRYEGID^{115}) upon SAM binding**. C)** Interaction map of TrmD (pink) in complex S-adenosyl homocysteine (SAH), PDB code 6NW7, shown as green stick representation. Hydrogen bonds, hydrophobic contacts, π-interactions are depicted in blue, red and black dotted lines respectively. **D)** Three representative fragment hits from each cluster, Fragment 14 (PDB Code 6QOK) coloured in blue, fragment 20 (PDB Code 6QOQ) in green and fragment 8 (PDB Code 6QOE) in salmon

respectively, occupying the TrmD cofactor site. Hydrogen bonds and electrostatic interactions are depicted in blue and green dotted lines respectively.

Figure 3: Fragment merging approach. **A)** Structural superposition of TrmD (grey) in complex with fragments **23** (beige) and **24** (light blue) – PDB Codes 6QOT & 6QOU, showing binding mode and interactions at the SAM site **B)** merged compound **AW1** (green), PDB Code 6QQS, and **C)** the overall scheme of fragment merging. **D)** Hot spot map contoured at 14 of TrmD active site superposed with crystal structure of TrmD in complex with merged compound AW1 (blue stick). Donor, acceptor and hydrophobic maps are depicted as blue, red and yellow regions respectively. Amino acid residues contributing towards interactions in each hotspot map region are shown as salmon lines. The arrows indicate two potential ways of fragment elaboration. **E)** X-ray crystal structure of TrmD (grey) in complex with initial merged compound AW1 (blue stick) showing binding mode at the SAM site. The corresponding amino acid interactions are illustrated with in dotted lines.

Figure 4: X-ray crystal structure of TrmD (grey) in complex with compounds in **A) AW2** (green stick), PDB Code 6QQX **(B) AW3** (yellow stick), PDB Code 6QQY **(C) AW5** at protomer 1, (blue stick), PDB Code 6QR6 and **(D) AW5** at protomer 2 (blue stick), PDB Code 6QR6, showing binding mode at the SAM site. The corresponding amino acid interactions are illustrated in dotted lines.

Figure 5: A) X-ray crystal structure of TrmD (grey) in complex with compound **A) AW6** (lime), PDB Code 6QR5 **B) AW7** (green), PDB Code 6QR8, showing binding mode at the SAM site. The corresponding amino acid interactions are illustrated with hydrogen bonds, π-interactions and ionic contacts depicted in blue, black and green dotted lines respectively. **C)**

Growth inhibition study of lead compounds **AW6** & **AW7** in *M. abscessus* infected human macrophages over a 48 h period. Data representative of three separate experiments. **D)** Percentage inhibition of intracellular *M. leprae* palmitic acid oxidation rate (radiorespirometry) in the presence of different concentrations of **AW7** for 7 days. 7th day cumulative counts per minute (CPM) were recorded and percentage inhibition of metabolism determined as compared to no drug control. **AW7** concentrations, in mM, are shown in parenthesis and rifampin (RMP) was used at 2.4 mM. * - Inhibition is statistically significant (P<0.05) compared to no drug control.

Table 1: Summary of structure guided optimization of merged compound AW1

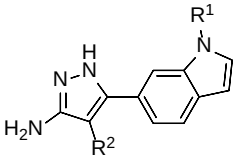

Compound	Structure		ΔT_m (°C)	K_d (µM)	LE (kcal/ heavy atom)	IC_{50} (µM)
	R^1	R^2				
AW1	**H**	**H**	+4.8	110 ± 10.0	0.36	226 ± 29.05
AW2	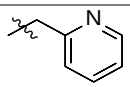	**H**	+3.1	12.3 ± 0.5	0.30	32.5 ± 3.99
AW3	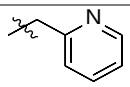	**CN**	+8.3	0.50 ± 0.14	0.36	0.31 ± 0.01
AW4	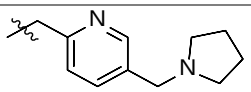	**CN**	+12.0	0.087 ± 0.02	0.32	ND
AW5	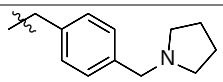	**CN**	+12.6	0.027 ± 0.007	0.34	0.03 ± 0.003
AW6	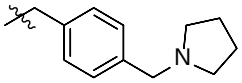	**H**	+7.8	0.49 ± 0.21	0.31	1.41 ± 0.074
AW7	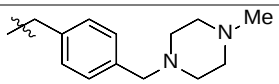	**CN**	+11.9	0.073 ± 0.03	0.30	0.069 ± 0.007

Table 2: Minimum inhibitory concentration (MIC) values of TrmD compounds across various mycobacterial species and strains

No	MIC (μM)							
	M. abscessus 19977	*M. tuberculosis Bluepan*	*M. tuberculosis* H37Rv #	*M. chelonae*	*M. fortuitum*	*M. gordonae*	*M. terrae*	*M. avium*
AW5	50.0	50.0	12.5	ND	ND	ND	ND	ND
AW6	50.0	25.0	6.25	100	100	100	100	200
AW7	50.0	25.0	6.25	100	100	100	25	100

 # Reported in (Whitehouse *et al.* 2019). *M. tuberculosis* H37Rv was grown in Middlebrook 7H9 base containing 14 mg/L dipalmitoyl phosphatidylcholine (DPPC), 0.81 g/L NaCl, 0.3 g/L casitone, and 0.05% Tyloxapol..

References

Adams, P.D., Afonine, P.V., Bunkoczi, G., Chen, V.B., Davis, I.W., Echols, N., Headd, J.J., Hung, L.W., Kapral, G.J., Grosse-Kunstleve, R.W., *et al.* (2010). PHENIX: a comprehensive Python-based system for macromolecular structure solution. Acta crystallographica Section D, Biological crystallography *66*, 213-221.

Ahn, H.J., Kim, H.W., Yoon, H.J., Lee, B.I., Suh, S.W., and Yang, J.K. (2003). Crystal structure of tRNA(m1G37)methyltransferase: insights into tRNA recognition. The EMBO journal *22*, 2593-2603.

Anantharaman, V., Koonin, E.V., and Aravind, L. (2002). SPOUT: a class of methyltransferases that includes spoU and trmD RNA methylase superfamilies, and novel superfamilies of predicted prokaryotic RNA methylases. J Mol Microbiol Biotechnol *4*, 71-75.

Bar-On, O., Mussaffi, H., Mei-Zahav, M., Prais, D., Steuer, G., Stafler, P., Hananya, S., and Blau, H. (2015). Increasing nontuberculous mycobacteria infection in cystic fibrosis. Journal of cystic fibrosis : official journal of the European Cystic Fibrosis Society *14*, 53-62.

Baugh, L., Phan, I., Begley, D.W., Clifton, M.C., Armour, B., Dranow, D.M., Taylor, B.M., Muruthi, M.M., Abendroth, J., Fairman, J.W., *et al.* (2015). Increasing the structural coverage of tuberculosis drug targets. Tuberculosis (Edinb) *95*, 142-148.

Bjork, G.R., Jacobsson, K., Nilsson, K., Johansson, M.J., Bystrom, A.S., and Persson, O.P. (2001). A primordial tRNA modification required for the evolution of life? The EMBO journal *20*, 231-239.

Bjork, G.R., Wikstrom, P.M., and Bystrom, A.S. (1989). Prevention of translational frameshifting by the modified nucleoside 1-methylguanosine. Science *244*, 986-989.

Christian, T., Sakaguchi, R., Perlinska, A.P., Lahoud, G., Ito, T., Taylor, E.A., Yokoyama, S., Sulkowska, J.I., and Hou, Y.M. (2016). Methyl transfer by substrate signaling from a knotted protein fold. Nat Struct Mol Biol *23*, 941-948.

DeJesus, M.A., Gerrick, E.R., Xu, W., Park, S.W., Long, J.E., Boutte, C.C., Rubin, E.J., Schnappinger, D., Ehrt, S., Fortune, S.M., *et al.* (2017). Comprehensive Essentiality Analysis of the Mycobacterium tuberculosis Genome via Saturating Transposon Mutagenesis. MBio *8*.

Emsley, P., and Cowtan, K. (2004). Coot: model-building tools for molecular graphics. Acta crystallographica Section D, Biological crystallography *60*, 2126-2132.

Erlanson, D.A., Fesik, S.W., Hubbard, R.E., Jahnke, W., and Jhoti, H. (2016). Twenty years on: the impact of fragments on drug discovery. Nature reviews Drug discovery *15*, 605-619.

Evans, P.R. (2011). An introduction to data reduction: space-group determination, scaling and intensity statistics. Acta crystallographica Section D, Biological crystallography *67*, 282-292.

Evans, P.R., and Murshudov, G.N. (2013). How good are my data and what is the resolution? Acta crystallographica Section D, Biological crystallography *69*, 1204-1214.

Floto, R.A., Olivier, K.N., Saiman, L., Daley, C.L., Herrmann, J.L., Nick, J.A., Noone, P.G., Bilton, D., Corris, P., Gibson, R.L., *et al.* (2016). US Cystic Fibrosis Foundation and European Cystic Fibrosis Society consensus recommendations for the management of non-tuberculous mycobacteria in individuals with cystic fibrosis. Thorax *71 Suppl 1*, i1-22.

Floyd, K., Glaziou, P., Zumla, A., and Raviglione, M. (2018). The global tuberculosis epidemic and progress in care, prevention, and research: an overview in year 3 of the End TB era. The Lancet Respiratory medicine *6*, 299-314.

Franzblau, S.G. (1988). Oxidation of palmitic acid by Mycobacterium leprae in an axenic medium. J Clin Microbiol *26*, 18-21.

French, S.W., K., (1978). On the treatment of negative intensity observations. Acta Cryst A34, 517-525.

Goto-Ito, S., Ito, T., Kuratani, M., Bessho, Y., and Yokoyama, S. (2009). Tertiary structure checkpoint at anticodon loop modification in tRNA functional maturation. Nat Struct Mol Biol *16*, 1109-1115.

Goto-Ito, S., Ito, T., and Yokoyama, S. (2017). Trm5 and TrmD: Two Enzymes from Distinct Origins Catalyze the Identical tRNA Modification, m(1)G37. Biomolecules *7*.

Griffin, J.E., Gawronski, J.D., Dejesus, M.A., Ioerger, T.R., Akerley, B.J., and Sassetti, C.M. (2011). High-resolution phenotypic profiling defines genes essential for mycobacterial growth and cholesterol catabolism. PLoS Pathog *7*, e1002251.

Hajduk, P.J., Huth, J.R., and Tse, C. (2005). Predicting protein druggability. Drug discovery today *10*, 1675-1682.

Hill, P.J., Abibi, A., Albert, R., Andrews, B., Gagnon, M.M., Gao, N., Grebe, T., Hajec, L.I., Huang, J., Livchak, S., *et al.* (2013). Selective inhibitors of bacterial t-RNA-(N(1)G37) methyltransferase (TrmD) that demonstrate novel ordering of the lid domain. Journal of medicinal chemistry *56*, 7278-7288.

Hodel, A., Kim, S.-H. & Brünger, A. T., (1992). Model bias in macromolecular crystal structures. Acta Cryst A *48*, 851-858.

Hori, H. (2017). Transfer RNA methyltransferases with a SpoU-TrmD (SPOUT) fold and their modified nucleosides in tRNA. Biomolecules *7*.

Ichihara, O., Shimada, Y., and Yoshidome, D. (2014). The importance of hydration thermodynamics in fragment-to-lead optimization. ChemMedChem *9*, 2708-2717.

Ito, T., Masuda, I., Yoshida, K., Goto-Ito, S., Sekine, S., Suh, S.W., Hou, Y.M., and Yokoyama, S. (2015). Structural basis for methyl-donor-dependent and sequence-specific binding to tRNA substrates by knotted methyltransferase TrmD. Proceedings of the National Academy of Sciences of the United States of America *112*, E4197-4205.

Kabsch, W. (2010). XDS. Acta crystallographica Section D, Biological crystallography *66*, 125-132.

Koh, C.S., Madireddy, R., Beane, T.J., Zamore, P.D., and Korostelev, A.A. (2017). Small methyltransferase RlmH assembles a composite active site to methylate a ribosomal pseudouridine. Scientific reports *7*, 969.

Kohanski, M.A., Dwyer, D.J., and Collins, J.J. (2010). How antibiotics kill bacteria: from targets to networks. Nat Rev Microbiol *8*, 423-435.

Lahiri, R., Randhawa, B., and Krahenbuhl, J. (2005). Application of a viability-staining method for Mycobacterium leprae derived from the athymic (nu/nu) mouse foot pad. J Med Microbiol *54*, 235-242.

Lahiri, R., Randhawa, B., and Krahenbuhl, J.L. (2010). Infection of mouse macrophages with viable Mycobacterium leprae does not induce apoptosis. J Infect Dis *201*, 1736-1742.

Li, G., Lian, L.L., Wan, L., Zhang, J., Zhao, X., Jiang, Y., Zhao, L.L., Liu, H., and Wan, K. (2013). Antimicrobial susceptibility of standard strains of nontuberculous mycobacteria by microplate Alamar Blue assay. PLoS One *8*, e84065.

Low, J.L., Wu, M.L., Aziz, D.B., Laleu, B., and Dick, T. (2017). Screening of TB Actives for Activity against Nontuberculous Mycobacteria Delivers High Hit Rates. Frontiers in microbiology *8*, 1539.

Lowe, T.M., and Chan, P.P. (2016). tRNAscan-SE On-line: integrating search and context for analysis of transfer RNA genes. Nucleic acids research *44*, W54-57.

Lowe, T.M., and Eddy, S.R. (1997). tRNAscan-SE: a program for improved detection of transfer RNA genes in genomic sequence. Nucleic acids research *25*, 955-964.

McCoy, A.J., Grosse-Kunstleve, R.W., Adams, P.D., Winn, M.D., Storoni, L.C., and Read, R.J. (2007). Phaser crystallographic software. J Appl Crystallogr *40*, 658-674.

Mendes, V., and Blundell, T.L. (2016). Targeting tuberculosis using structure-guided fragment-based drug design. Drug discovery today.

Murray, C.W., Erlanson, D.A., Hopkins, A.L., Keseru, G.M., Leeson, P.D., Rees, D.C., Reynolds, C.H., and Richmond, N.J. (2014). Validity of ligand efficiency metrics. ACS medicinal chemistry letters *5*, 616-618.

Murshudov, G.N., Skubak, P., Lebedev, A.A., Pannu, N.S., Steiner, R.A., Nicholls, R.A., Winn, M.D., Long, F., and Vagin, A.A. (2011). REFMAC5 for the refinement of macromolecular crystal structures. Acta crystallographica Section D, Biological crystallography *67*, 355-367.

Radoux, C.J., Olsson, T.S., Pitt, W.R., Groom, C.R., and Blundell, T.L. (2016). Identifying Interactions that Determine Fragment Binding at Protein Hotspots. Journal of medicinal chemistry *59*, 4314-4325.

Sampson, S.L., Dascher, C.C., Sambandamurthy, V.K., Russell, R.G., Jacobs, W.R., Jr., Bloom, B.R., and Hondalus, M.K. (2004). Protection elicited by a double leucine and pantothenate auxotroph of Mycobacterium tuberculosis in guinea pigs. Infect Immun *72*, 3031-3037.

Sassetti, C.M., Boyd, D.H., and Rubin, E.J. (2003). Genes required for mycobacterial growth defined by high density mutagenesis. Mol Microbiol *48*, 77-84.

Scherr, N., Pluschke, G., and Panda, M. (2016). Comparative Study of Activities of a Diverse Set of Antimycobacterial Agents against Mycobacterium tuberculosis and Mycobacterium ulcerans. Antimicrob Agents Chemother *60*, 3132-3137.

Shepard, C.C., and McRae, D.H. (1968). A method for counting acid-fast bacteria. Int J Lepr Other Mycobact Dis *36*, 78-82.

Sood, G., and Parrish, N. (2017). Outbreaks of nontuberculous mycobacteria. Curr Opin Infect Dis *30*, 404-409.

Thomas, S.E., Mendes, V., Kim, S.Y., Malhotra, S., Ochoa-Montano, B., Blaszczyk, M., and Blundell, T.L. (2017). Structural Biology and the Design of New Therapeutics: From HIV and Cancer to Mycobacterial Infections: A Paper Dedicated to John Kendrew. Journal of molecular biology *429*, 2677-2693.

Truman, R.W., and Krahenbuhl, J.L. (2001). Viable M. leprae as a research reagent. Int J Lepr Other Mycobact Dis *69*, 1-12.

Urbonavicius, J., Qian, Q., Durand, J.M., Hagervall, T.G., and Bjork, G.R. (2001). Improvement of reading frame maintenance is a common function for several tRNA modifications. The EMBO journal *20*, 4863-4873.

Vonrhein, C., Flensburg, C., Keller, P., Sharff, A., Smart, O., Paciorek, W., Womack, T., and Bricogne, G. (2011). Data processing and analysis with the autoPROC toolbox. Acta crystallographica Section D, Biological crystallography *67*, 293-302.

Whitehouse, A.J., Thomas, S.E., Brown, K., Fanourakis, A., Libardo, M.D.J., Chan, D.S.H., Mendes, V., Boshoff, H.I.M., Floto, R.A., Abell, C., Blundell, T.L., Coyne, A.G. Development of inhibitors against Mycobacterium abscessus tRNA (m^1G37) methyltransferase (TrmD) using fragment-based approaches.

Winn, M.D., Ballard, C.C., Cowtan, K.D., Dodson, E.J., Emsley, P., Evans, P.R., Keegan, R.M., Krissinel, E.B., Leslie, A.G., McCoy, A., *et al.* (2011). Overview of the CCP4 suite and current developments. Acta crystallographica Section D, Biological crystallography *67*, 235-242.

Zhong, W., Koay, A., Ngo, A., Li, Y., Nah, Q., Wong, Y.H., Chionh, Y.H., Ng, H.Q., Koh-Stenta, X., Poulsen, A., *et al.* (2019). Targeting the Bacterial Epitranscriptome for Antibiotic Development: Discovery of Novel tRNA-(N(1)G37) Methyltransferase (TrmD) Inhibitors. ACS infectious diseases.

Author Contributions

RAF, TLB., VM., AC and CA conceived and managed the project. SET, AJW and VM wrote the manuscript and designed the experiments. SET and PG performed the molecular biology and expression, protein purification, characterization, crystallography and fragment library screening. AC, CA and AJW modelled and designed the compounds. AJW synthesized and characterised the compounds. SET and AJW performed the biophysical and biochemical assays. KPB performed the microbiological experiments on *M. abscessus, M. tuberculosis* and NTMs. MDJL performed the microbiological experiments on *M. tuberculosis* H37Rv. MJ and JMB designed and carried out the *trmD* knockout studies. RL designed and performed the experiments on *M. leprae.* SM did the bioinformatics studies and t-RNA sequence searches. DJL and HIMB performed MIC determinations on *M. tuberculosis H37Rv.*

Acknowledgements

This work is funded by the Cystic Fibrosis Trust (Registered as a charity in England and Wales (1079049) and in Scotland (SC040196) Strategic research consortium and in part by the Intramural Research Program of the NIH, NIAID. The authors would like to thank the Diamond Light Source for beam-time (proposals mx9537, mx14043, mx18548) and the staff of beamlines I03, I02, I04, I04-1 and I24 for assistance with data collection, the Seattle Structural Genomics Consortium for kindly providing the *M. abscessus trmD* AVA0421 plasmid, Prof. Ben Luisi and Dr. Kasia J. Bandrya (Department of Biochemistry, University of Cambridge) for insights on experimental design using tRNA, Dr. Sundeep Chaitanya for discussions on *M. leprae* inhibition studies. SET is funded by the Cystic Fibrosis Trust (RG 70975) and

Foundation Botnar (RG91317); VM is funded by the Bill and Melinda Gates Foundation SHORTEN-TB (RG 86546); TLB is funded by the Wellcome Trust (Wellcome Trust Investigator Award 200814_Z_16_Z: RG83114). AW is funded through the EPSRC. RAF, TLB and CA would like to thank the Fondation Botnar for funding (Grant No. RG91317).

Competing Interests

There are no competing interests

Accession Numbers

Coordinates and structure factors related to this work been deposited in the PDB with accession numbers 6NVR, 6NW6, 6NW7, 6QO2, 6QO3,6QO4, 6QO6, 6QOA, 6QOC, 6QOD, 6QOE, 6QOF, 6QOG, 6QOH, 6QOI, 6QOJ, 6QOK, 6QOL, 6QOM, 6QON, 6QOO, 6QOP, 6QOQ, 6QOR, 6QOS, 6QOT, 6QOU, 6QOV, 6QOW, 6QOX, 6QQS, 6QQX, 6QQY, 6QR6, 6QR5 and 6QR8.

Materials & Correspondence

Correspondence for materials should be addressed to V.M. and T.L.B.

Figure 1

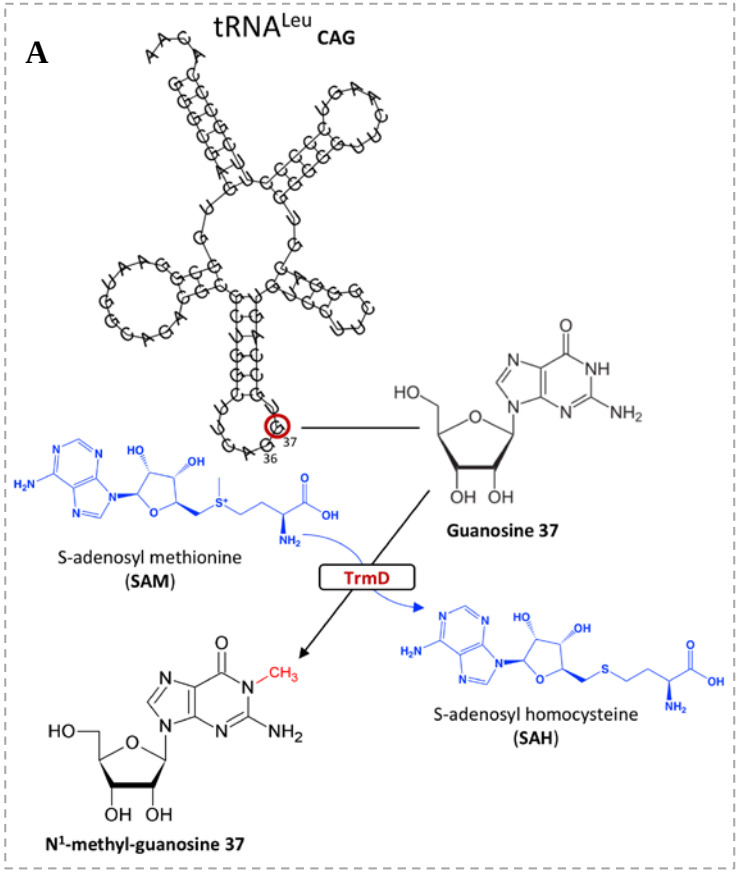
A
tRNA$^{Leu}_{CAG}$
37
36
Guanosine 37
S-adenosyl methionine
(SAM)
TrmD
S-adenosyl homocysteine
(SAH)
N^1-methyl-guanosine 37

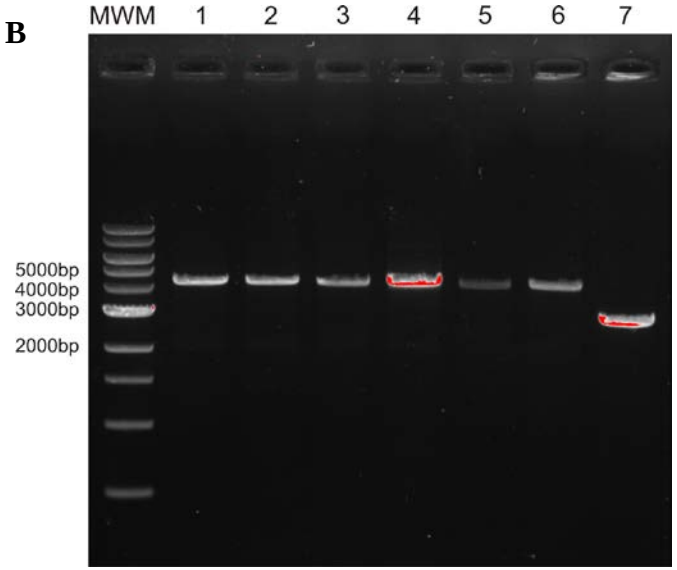
B
MWM
1
2
3
4
5
6
7
5000bp
4000bp
3000bp
2000bp

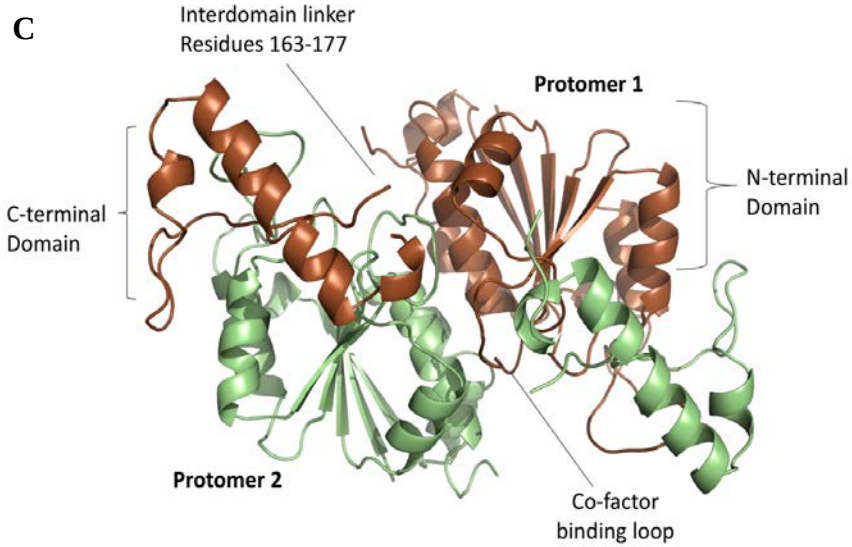
C
Interdomain linker
Residues 163-177
Protomer 1
C-terminal
Domain
N-terminal
Domain
Protomer 2
Co-factor
binding loop

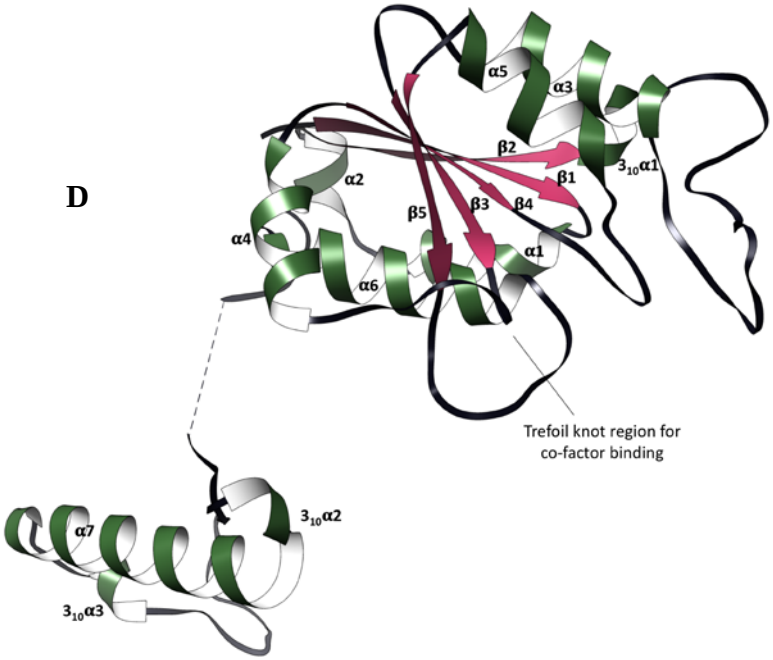
D
α5
α3
β2
β1
3_{10}α1
α2
β5
β3
β4
α4
α1
α6
Trefoil knot region for
co-factor binding
α7
3_{10}α2
3_{10}α3

Figure 2

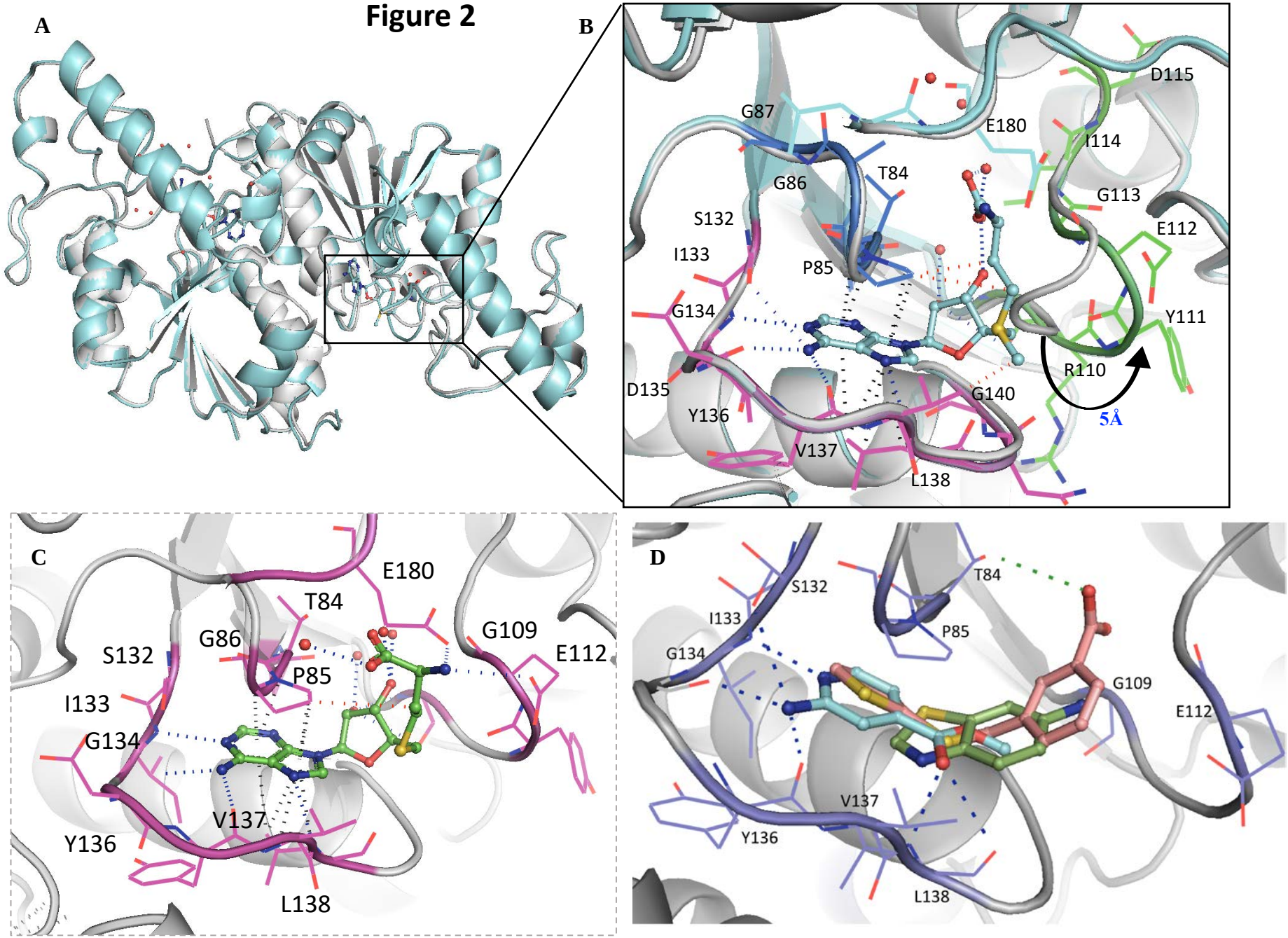
A
B
G87
E180
D115
I114
T84
G86
G113
S132
E112
I133
P85
G134
Y111
R110
D135
G140
Y136
5Å
V137
L138
C
E180
T84
G86
G109
S132
E112
P85
I133
G134
V137
Y136
L138
D
S132
T84
I133
P85
G134
G109
E112
V137
Y136
L138

Figure 3

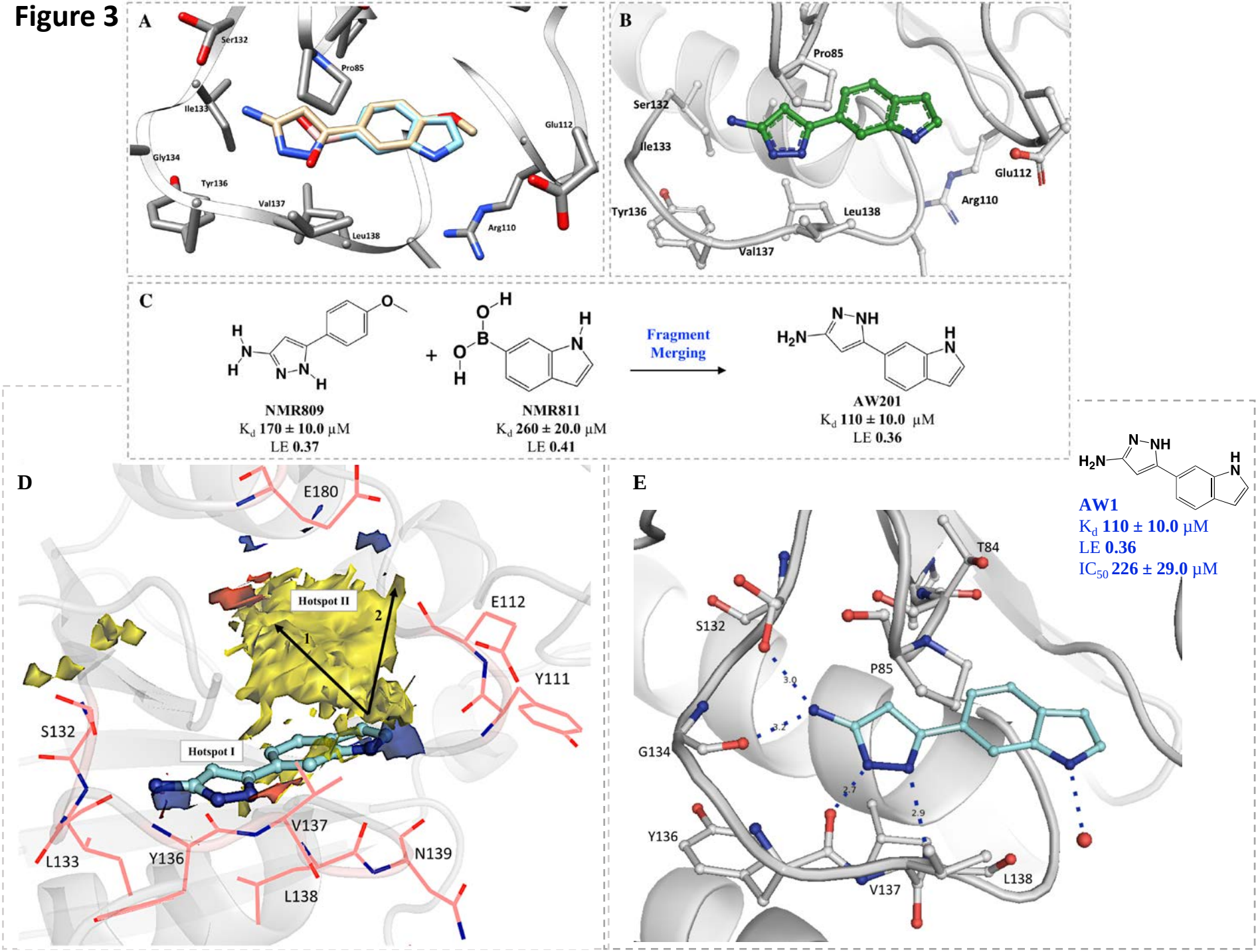
A
Ser132
Pro85
Ile133
Gly134
Tyr136
Val137
Leu138
Glu112
Arg110
B
Pro85
Ser132
Ile133
Tyr136
Val137
Leu138
Glu112
Arg110
C
NMR809
Kd 170 ± 10.0 μM
LE 0.37
NMR811
Kd 260 ± 20.0 μM
LE 0.41
Fragment Merging
AW201
Kd 110 ± 10.0 μM
LE 0.36
D
E180
Hotspot II
Hotspot I
E112
Y111
S132
L133
Y136
V137
L138
N139
E
AW1
Kd 110 ± 10.0 μM
LE 0.36
IC50 226 ± 29.0 μM
T84
S132
P85
G134
Y136
V137
L138

Figure 4

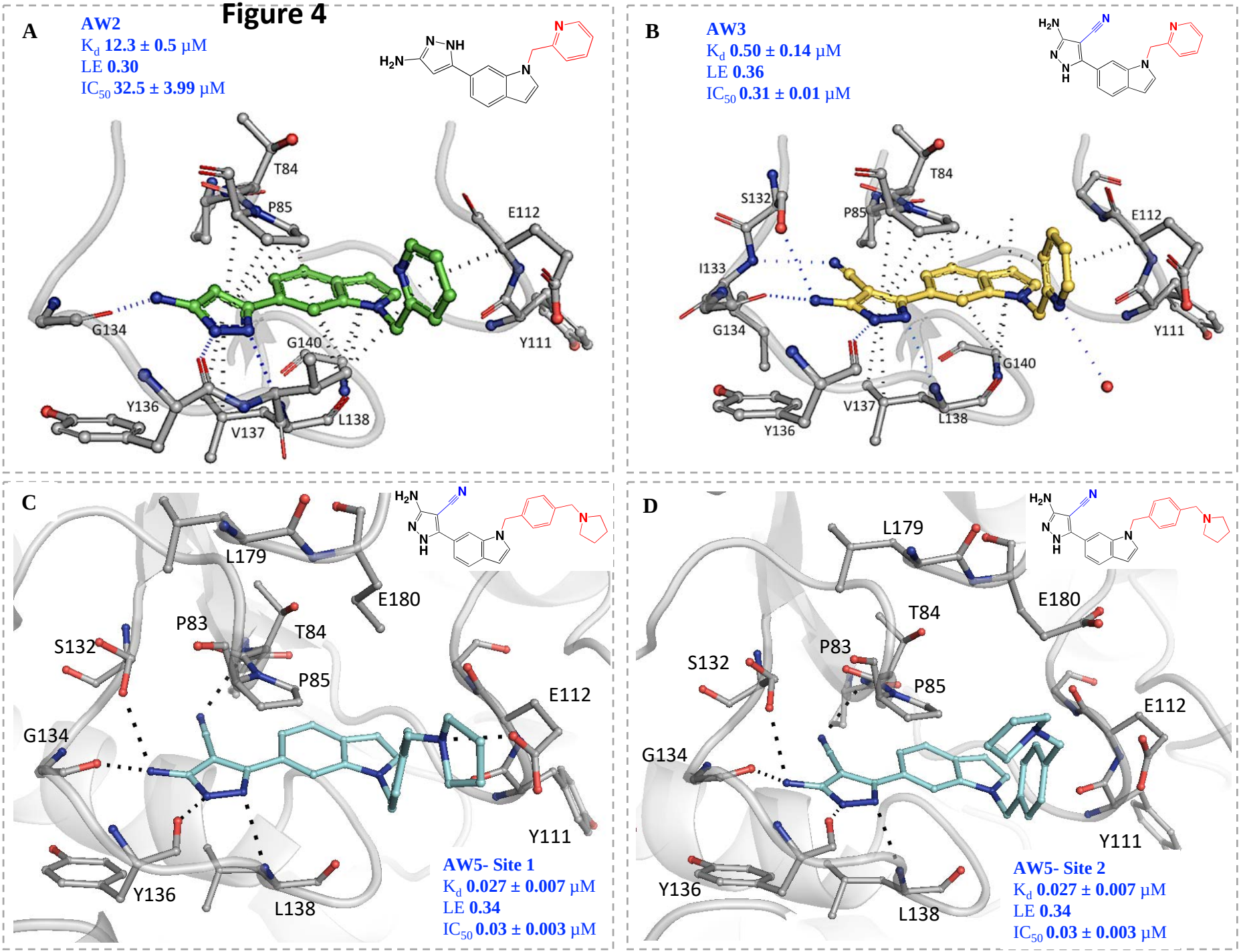
A
AW2
K_d 12.3 ± 0.5 μM
LE 0.30
IC_{50} 32.5 ± 3.99 μM
T84
P85
E112
G134
G140
Y111
Y136
V137
L138
B
AW3
K_d 0.50 ± 0.14 μM
LE 0.36
IC_{50} 0.31 ± 0.01 μM
S132
T84
P85
E112
I133
G134
Y111
G140
V137
L138
Y136
C
L179
E180
P83
T84
S132
P85
E112
G134
Y111
Y136
L138
AW5- Site 1
K_d 0.027 ± 0.007 μM
LE 0.34
IC_{50} 0.03 ± 0.003 μM
D
L179
E180
T84
P83
S132
P85
E112
G134
Y111
Y136
L138
AW5- Site 2
K_d 0.027 ± 0.007 μM
LE 0.34
IC_{50} 0.03 ± 0.003 μM

Figure 5

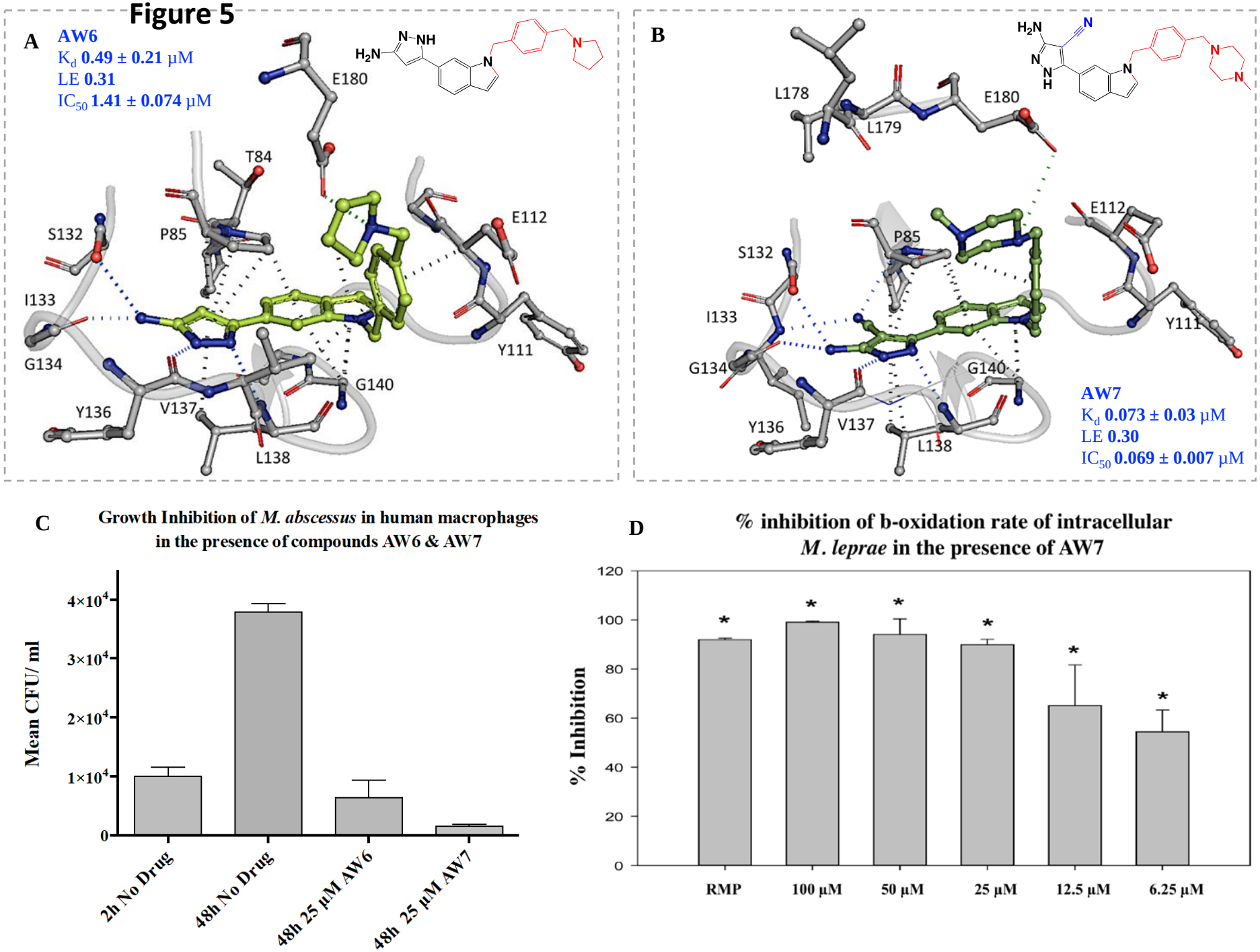
A
AW6
K_d 0.49 ± 0.21 μM
LE 0.31
IC_{50} 1.41 ± 0.074 μM
E180
T84
S132
P85
E112
I133
G134
Y111
G140
Y136
V137
L138
B
L178
L179
E180
E112
S132
P85
I133
Y111
G134
G140
Y136
V137
L138
AW7
K_d 0.073 ± 0.03 μM
LE 0.30
IC_{50} 0.069 ± 0.007 μM
C
Growth Inhibition of M. abscessus in human macrophages in the presence of compounds AW6 & AW7
Mean CFU/ ml
4×10⁴
3×10⁴
2×10⁴
1×10⁴
0
2h No Drug
48h No Drug
48h 25 μM AW6
48h 25 μM AW7
D
% inhibition of b-oxidation rate of intracellular M. leprae in the presence of AW7
% Inhibition
120
100
80
60
40
20
0
RMP
100 μM
50 μM
25 μM
12.5 μM
6.25 μM